Ceramics International 45 (2019) 12455–12460

Contents lists available at ScienceDirect

Ceramics International

journal homepage: www.elsevier.com/locate/ceramint

Residual mechanical stresses in pressure treated $BaTiO_3$ powder

I.V. Zaytseva[a], A.M. Pugachev[a], K.A. Okotrub[a], N.V. Surovtsev[a], S.L. Mikerin[a], A.S. Krylov[b,*]

[a] Institute of Automation and Electrometry SB RAS, Novosibirsk, 630090, Russia
[b] Kirensky Institute of Physics Federal Research Center KSC SB RAS, Krasnoyarsk, 660036, Russia

ARTICLE INFO

Keywords:
Residual mechanical stress
Raman spectroscopy
High non-hydrostatic pressure
Temperature treatment
Residual pressure
$BaTiO_3$ ceramics

ABSTRACT

Here we present Raman spectroscopy approach to monitor the spatial distribution and the magnitude of the residual mechanical stresses in ceramic after non-hydrostatic pressure treatments. The residual pressure can be found from the E-phonon line shift ($\sim 307\ cm^{-1}$) in the Raman spectra. The relationship between the non-hydrostatic pressure (up to 11 GPa) and the shift of this line has been established. It is demonstrated that the change in the Raman line position ($1332\ cm^{-1}$) of the diamond anvil can be used for monitoring of applied non-hydrostatic pressures. A linear dependence of residual mechanical stresses on the applied pressures is found. Micro-Raman spectroscopy shows that the residual mechanical stresses are distributed fairly uniformly in the studied $BaTiO_3$ samples at the micron scale. In the future, the proposed Raman technique can be used for monitoring the quality of produced $BaTiO_3$ ceramics.

1. Introduction

The non-hydrostatic pressure treatment of the ferroelectric powders is widely used in the manufacture of ferroelectric ceramics. While most studies of pressure effects on ferroelectric powders are devoted to a case of hydrostatic pressure treatment, which is well described theoretically and experimentally [1–3], effects of the non-hydrostatic pressure treatment may differ significantly. The shift of the phase transition temperature in $BaTiO_3$ powders is known to decrease under hydrostatic pressure [4] in contrast to its behaviour in $BaTiO_3$ powders under non-hydrostatic pressure. It was shown that residual mechanical stresses inside the pressure treated samples (mechanical stresses after removal of external non-hydrostatic ones) lead to increase of the temperature and width of the ferroelectric phase transition from cubic to tetragonal phase [5–8]. It was proposed that a random distribution of residual stresses and associated random electric fields leads to relaxor-like properties of pressure-treated powders [9].

Dependence of the ferroelectric phase transition temperature T_C on the pressure was investigated earlier [10]. The hydrostatic pressure leads to a decrease of T_C in crystals and ceramic with the rate of about 5 °C/kBar [11]. It is confirmed by various experiments [12–15] and theoretical works [16,17]. At the same time, it was experimentally evidenced that the phase transition temperature increases under uniaxial pressing below 0.5 GPa [18,19]. The possibility of increasing the temperature T_C at uniaxial pressure was also considered in Ref. [20]. The application of uniaxial mechanical stress to $BaTiO_3$ causes to reorientation of domains in the direction perpendicular to the applied load by the ferroelastic effect. It was confirmed in Ref. [19] by dielectric measurements: authors observed an increase in permittivity for the stressed crystals. This increase in permittivity is consistent with the known anisotropy of the permittivity in tetragonal $BaTiO_3$ along the *c*- and *a*-axes. Here *c* and *a* are lattice constants along and perpendicular polar axis respectively. In this way, uniaxial mechanical stress increases the density of domain (and dipole momentum respectively) in a certain direction in originally unpolarized ceramics. This, in turn, increases the ferroelectric phase transition temperature.

The shift of T_c, with pressure, should obey the Clausius-Clapeyron equation [11]:

$$\frac{dT_c}{dp} = T_c \frac{\Delta V}{L}$$

where p is the pressure and ΔV and L are the difference between volumes of the unit cell in ferroelectric and paraelectric phase and latent heat, respectively.

The value of ΔV in unstressed ceramic could predict the slope of dT/dp, however, X-ray investigations of lattice constants did not demonstrate a change in this value upon the ferroelectric phase transition in barium titanate if $p = 0$ [21–23]: the values of *c* decrease, and *a* increase while the value of $\Delta V = a^2 * c$ does not change with the accuracy of experiments. We can conclude that the application of the external pressure leads to both reduction and increase of the volume of the unit cell for hydrostatic and nonhydrostatic pressures respectively.

* Corresponding author.
E-mail address: shusy@iph.krasn.ru (A.S. Krylov).

https://doi.org/10.1016/j.ceramint.2019.03.179
Received 5 December 2018; Received in revised form 6 March 2019; Accepted 24 March 2019
Available online 25 March 2019

In addition, the temperature behaviour of the paraelectric to a ferroelectric phase transition in $BaTiO_3$ powders under non-hydrostatic pressure is similar to that in thin strained $BaTiO_3$ films grown on different substrates due to the existence of enormous strains [24–26].

Raman spectroscopy is a convenient method for measurements of residual mechanical stress. In the case of $BaTiO_3$, E-phonon narrow line near 307 cm^{-1} in the Raman spectra (E(TO) line) can be used for such measurements because a mechanical stress causes a shift of this Raman line [27,28].

Luminescence technique is actively used for a high-pressure measurement in hydrostatic experiments. The applied pressures could be monitored by shifting the $^5D_0$-$^7F_0$ fluorescence band of the Sm^{2+} ion in the SrB_4O_7: Sm^{2+} crystal [29–31]. Nevertheless, the non-hydrostatic applied pressures result in broadening and splitting into a set of two or more lines of the fluorescence band of the Sm^{2+} ion. Moreover, a spatial inhomogeneity of the position of $^5D_0$-$^7F_0$ fluorescence band of the Sm^{2+} ion under non-hydrostatic pressing was obtained in Ref. [29]. Simultaneously the E(TO) line position in the Raman spectra of $BaTiO_3$ powder remained unchanged in the field of illumination. Consequently, SrB_4O_7: Sm^{2+} crystal is not a good sensor for monitoring non-hydrostatic pressures in case of powders.

Thus, the problem of non-hydrostatic pressure calibration is an actual task required for various pressure treatment applications.

Another advantage of Raman spectroscopy is the capability to characterize the materials with high spatial resolution. In the case of ceramics formed from powder, separate grains in the powder stick together under the pressuring forming non-uniform polycrystalline structure. Thus, the homogeneity of residual mechanical stress is the important property of ceramic material. Raman mapping can be used to reveal possible microscopic inhomogeneities in $BaTiO_3$ ceramics.

This paper aims to propose the technique for evaluating and monitoring of the magnitude and spatial distribution of residual mechanical stresses in $BaTiO_3$ powders treated by non-hydrostatic pressures.

2. Materials and methods

High-pressure experiments were carried out in EasyLab μScope DAC- HT(G) (UK) in nominally pure $BaTiO_3$ powder (Aldrich) with a grain size less than 2 μm. The Raman spectra of $BaTiO_3$ powder under high pressure were recorded at room temperature (296 K). In these experiments, the liquid pressure transmittance media was not used. Consequently, the non-hydrostatic pressing was realised.

Raman spectra were measured in a backscattering geometry. The laser beam was focused on the sample, and scattered light was collected by with a 50 × Olympus LMPlanFl objective lens with N.A. = 0.35. Raman spectra were excited by the Ar^+ ion laser Spectra-Physics Stabilite 2017 with λ = 514.5 nm and power of 5 mW. Spectra of scattered light were recorded by the triple T64000 Horiba Jobin Yvon spectrometer.

The schematic drawing of the experimental setup is presented in Fig. 1. The stainless steel gasket was pre-indented at 15 GPa with a 500 μm culets from an initial thickness of 250 to 86 μm. The entire 500 μm indentation was drilled out with an electric discharge machine by 200 μm diameter WC electrode. $BaTiO_3$ powder together with small SrB_4O_7:Sm^{2+} crystal was placed in the hole.

The Raman mapping of these samples was carried out using a laboratory-built experimental setup [32]. A solid-state laser (Millennia II; Spectra Physics) with λ = 532.1 nm and a 100 × objective (PL Fluotar L; Leica Microsystems, Wetzlar, Germany) with NA = 0.75 were used. The irradiation power after objective was 16 mW.

The sample pellets with a diameter of 5 mm were prepared by non-hydrostatic pressing of $BaTiO_3$ powders (values of pressures ranged up to 4 GPa) to study spatial distributions of the residual mechanical stresses using Raman spectroscopy. Several $BaTiO_3$ pellets were annealed at the temperature of 900 °C during the various time to reduce the magnitude of residual mechanical stresses. The reference $BaTiO_3$ crystal used in the experiment was grown by the top-seeded solution growth method. This crystal was cut in the form of (100)-oriented plate, which was polished to optical quality (it is denoted as sample 1). The samples under study, namely the powder of barium titanate and the same powder subjected to non-hydrostatic pressing under 4 GPa, are designated as samples 2 and 4, respectively. The sample treated by non-hydrostatic pressing under 4 GPa and annealed at 900 °C during 30 min, is denoted as sample 3.

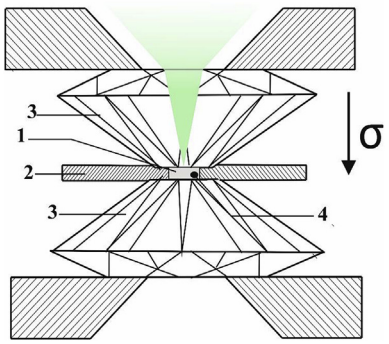

Fig. 1. Schematic drawing of the experimental setup: 1. $BaTiO_3$ powder; 2. the steel gasket; 3. the diamond anvils; 4. the SrB_4O_7: Sm^{2+} crystal.

3. Results and discussion

3.1. Evaluation of applied non-hydrostratic pressures in the diamond anvil cell

Since the reproducible measurement of applyed non-hydrostatic pressures using fluorescence of SrB_4O_7: Sm^{2+} crystal is problematic, we studied Raman spectra of a diamond anvil for monitoring the pressure applied to $BaTiO_3$ samples. The possibility of the measurement of mechanical stresses by monitoring the shift of the Raman line (1332 cm^{-1}) in the diamond anvil was demonstrated earlier [33–36]. It is well known that pressure leads to a distribution of mechanical stresses along the diamond anvil axis [35]. Thus we used the confocal microscopy, for measurements of Raman spectra in the diamond anvil from a region near the center of the culet face of the diamond. The experiment showed that the position of the diamond peak does not depend on the position of the point on the sample surface in the region of the gasket hole.

To relate the Raman line position of the diamond anvil and applied non-hydrostatic pressure, a calibration experiment with hydrostatic pressures was carried out. In this case, we added the water to the gasket hole and placed SrB_4O_7: Sm^{2+} crystal. Fig. 2 shows the position of Raman lines in the diamond anvil as the function of applied hydrostatic mechanical stresses. The magnitudes of these mechanical stresses were calculated through the shift of the ^{5}D0-^{7}F0 fluorescence band of the Sm^{2+} ion [31].

Raman spectrum of the unstressed diamond represents the single line near 1332 cm^{-1}. This phonon state is triply degenerated, and degeneration is reduced by applied pressure [36]. Also, there is a shift of the line position under pressure. The inset in Fig. 2 demonstrates that the Raman line in the diamond anvil splits into three lines under pressure (a spectral shape of the Raman line under pressure was fitted by a sum of three Lorentzians).

The frequencies of three components increases linearly as applied pressure increases. It is worthwhile to clarify that the linear behaviour of the positions of these peaks was also observed in our non-hydrostatic experiments.

For the value of pressure evaluation, we used the position of the high -frequency line. The pressure dependence is described by the linear function

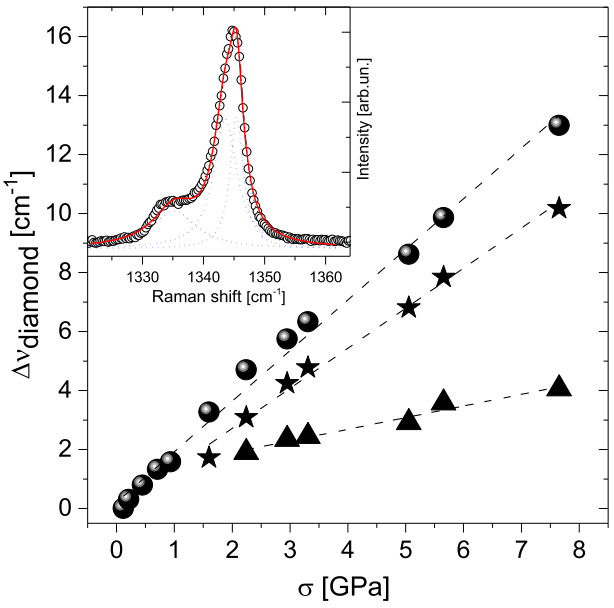

Fig. 2. The Raman line position of the diamond anvil relative to its initial position (1332 cm^{-1}) near the surface of the sample *versus* hydrostatic pressures. The circles, stars, and triangles correspond to the positions of different components of the Raman spectrum in the diamond anvil. The straight lines are linear fits of the pressure dependence for these frequency edges. The inset demonstrates the Raman line in the diamond anvil under the applied pressure of 6 GPa. The solid line is the fit of the experimental spectrum by a sum of three Lorentzians, and short dotted lines are the Lorentzian contours.

$$\Delta\nu_{DAC} \approx 0.57\left[\frac{cm^{-1}}{GPa}\right] * \sigma \quad (1)$$

where $\Delta\nu_{DAC}$- the difference of the position of the maximum relative to its initial position (1332 cm^{-1}), σ [GPa] – applied mechanical stress. The obtained result can be used for the evaluation of the non-hydrostatic mechanical stresses.

3.2. The shift of the Raman line as a tool for measurement of mechanical stresses in the pressed powder

The Raman spectra of $BaTiO_3$ powder were measured under non-hydrostatic pressures up to 11 GPa. The magnitudes of applied non-hydrostatic pressures were determined by Eq (1) through the Raman line position in the diamond anvil. These measurements confirm the results [29] when E(TO) line is shifted to higher frequencies with increasing pressure: $\nu_{E(TO)} = \nu_0 + \Delta\nu_{E(TO)}$. The symbol $\Delta\nu_{E(TO)}$ denotes the difference between the position of the E(TO) Raman line in the powder under the action of applied pressure and the position of this line in the same powder without pressure (ν_o). The dependence of the values of $\Delta\nu_{E(TO)}$ on the applied non-hydrostatic pressures is shown in Fig. 3 (a).

The linear part of the $\Delta\nu_{E(TO)}$ dependence on the applied non-hydrostatic pressures can be described by the function

$$\Delta\nu_{E(TO)} = \xi * \sigma \quad (2)$$

Where

$$\xi \approx 0.9\left[\frac{GPa}{cm^{-1}}\right].$$

It should be noted that the E-phonon line near 307 cm^{-1} which is a characteristic feature of the tetragonal (ferroelectric) phase [37] is manifested for all pressure range (see also the inset ib Fig. 3). This fact points out that the $BaTiO_3$ powder does not undergo the ferroelectric phase transition from tetragonal to cubic phase under non-hydrostatic

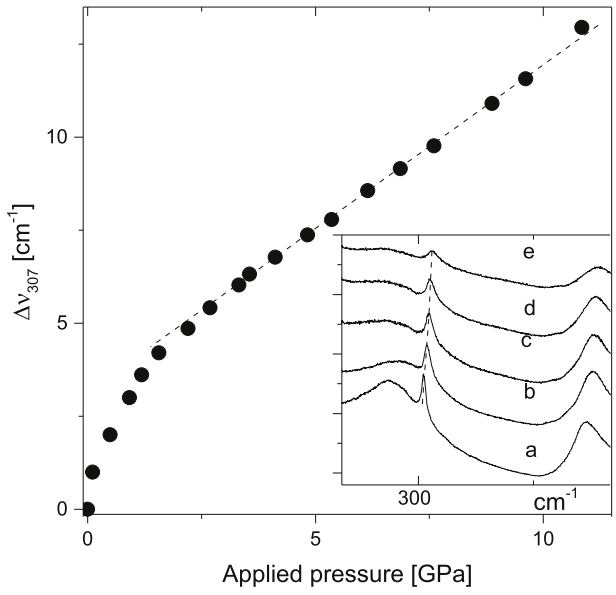

Fig. 3. (a) *the* $\Delta\nu_{E(TO)}$*versus a non-hydrostatic pressure. The dashed line corresponds to Eq. (2). Typical Raman spectra under different non-hydrostatic pressures at room temperature are demonstrated in the inset. A corresponds to non-pressed powder, b – e – to the same powder under a non-hydrostatic pressures of 3.5, 6.5, 8.3,* 11 GPa *respectively.*

pressures up to 11 GPa. On the contrary, the hydrostatic pressure application more than 2 GPa applied to $BaTiO_3$ powder leads the transition into the cubic phase [38].

3.3. Residual mechanical stresses in $BaTiO_3$ powder treated by non-hydrostatic pressure and temperature annealing at 900 °C. Their magnitudes and spatial distribution

Residual mechanical stresses were determined by the value $\Delta\nu_{E(TO)}$ with the help of Eq. (2).

The micro-Raman experiments were carried out to obtain the distribution of mechanical stresses remaining in powders after pressure and temperature treatment. The Raman mapping of the crystal, untreated powder, pressure and temperature treated powders of $BaTiO_3$ were carried out on an area of 30 × 30 μm with a spatial resolution about 0.6 μm at room temperature. This mapping is demonstrated in Fig. 4.

Fig. 5 (a) demonstrates the distributions of a number of micro-regions with the same values of the position of the E(TO) Raman line (N) in the crystal (1), untreated powder (2), pressure treated (4), pressure and temperature treated powders of $BaTiO_3$.

The samples under study differ from each other by the E(TO) line position. The nature of the difference between the distributions of $\nu_{E(TO)}$ position in the crystal and unstressed powder is unknown now. The difference between the distribution of $\nu_{E(TO)}$ positions in samples 3 and 4 relative to unstressed powder seem to be caused by the residual mechanical stresses acting in the samples after pressure treatment and annealing of sample 4, which decrease residual mechanical stresses.

Distributions of *N* in all samples are symmetric and correspond to the Gaussian. Most likely, the FWHM of this distribution for the crystal (~0.17 cm^{-1}) is determined not by the actual spreading of mechanical stresses in the crystal bulk, but by the accuracy of our experiment. FWHM of the distribution in unstressed powder is about 0.22 cm^{-1}. Errors of measurements may cause the minor broadening of N in the powder relative to the crystal due to spatial inhomogeneities in the micron and submicron powder. The FWHM of *N* in the samples 3 and 4 are similar to the sample 2. Therefore, despite the dispersion of these values obtained in the experiment, it can be concluded that the residual

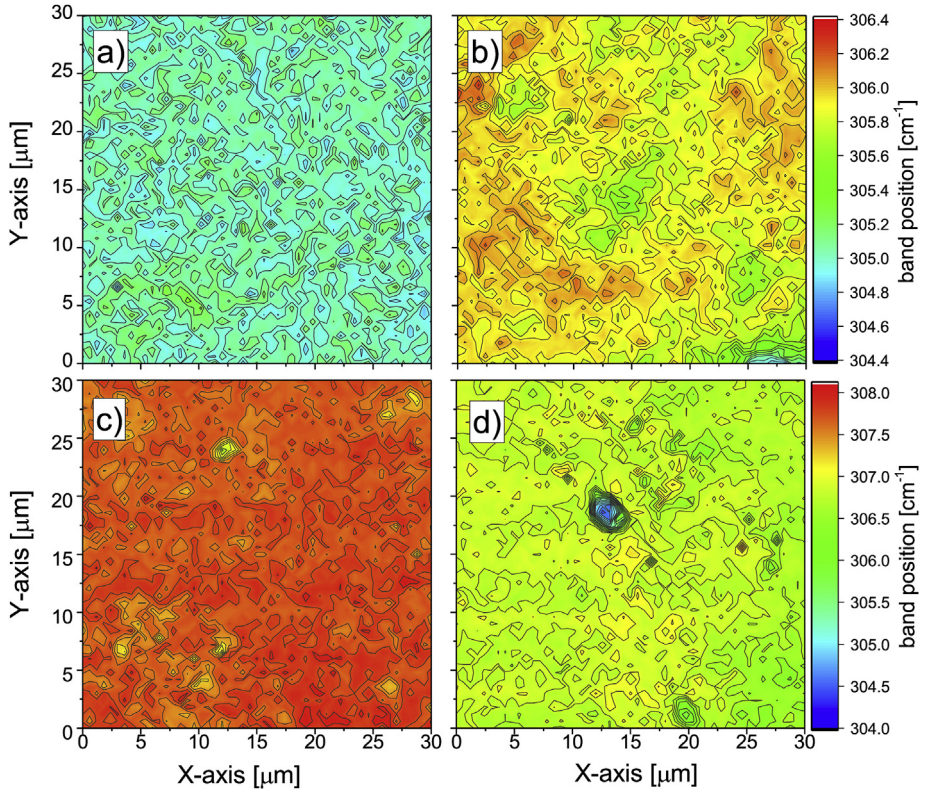

Fig. 4. The Raman mapping of a) the crystal; b) untreated powder; c) pressure, d) pressure and temperature treated powders of $BaTiO_3$. These measurements were carried out on an area of 50 * 50 points with a spatial resolution about 0.6 μm.

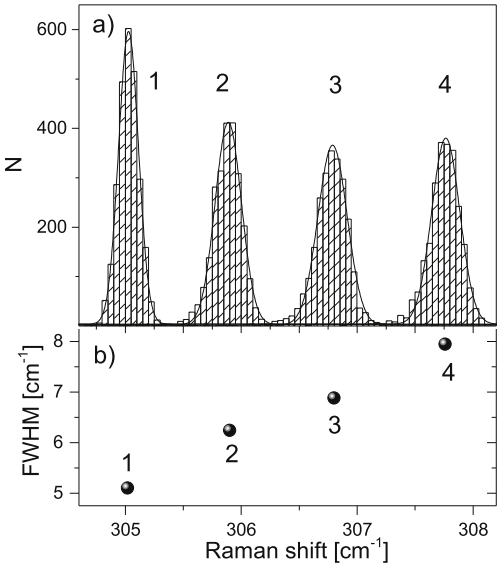

Fig. 5. (a) The distribution of the E(TO) Raman line position for the samples 1–4. The solid lines represent Gaussian fits to the experimental data. Here N is a number of microregions with the same values of the E(TO) line position. (b) The FWHM dependence of the E(TO) line position vs their position for the samples 1–4.

mechanical stresses acting in the volume of the pressed powder are distributed relatively uniformly in the micron scale.

The applied uniaxial pressure formed the microstructure depicted in Fig. 6. These images were obtained by Scanning electron microscope Hitachi TM 3000 due to the emission of secondary electrons from a gilded surface (the thickness of the gold layer is about 30 nm), U = 15 kV.. The powder consists of grains less than 100 nm held to each other, most likely, by electrostatic forces. Clearly distinguishable grains of size about 100–300 nm appear after pressing by 4 GPa (Fig. 6c and 6d). Temperature annealing at 900 °C for 30 min does not change the picture (Fig. 6e and f). Local mechanical stresses acting in the sample do not change both the size and location of the grains.

The FWHM of the E(TO) Raman line near 307 cm^{-1} was investigated. For this purpose, all the spectra measured during the scan were averaged and fitted this Raman line by the Voigt contour (the procedure of this fitting was described in Ref. [9] in detail). The exact Raman line width (Lorentz part of the contour) in the samples 1–4 differs from each other. It depends on the line position (see Fig. 5 (b)). Inhomogeneous broadening of this Raman line may be associated with a shortening of the corresponding lifetimes of vibration states. On the other hand, it may be caused by the appearance of defect states in samples 2–4 due to the treatment of the powder: the grinding, application of mechanical stresses and temperature annealing. Such inhomogeneous broadening can occur on much smaller scales, up to atomic [39].

4. Conclusion

The technique justification how to evaluate and monitor the magnitude and spatial distribution of residual mechanical stresses in $BaTiO_3$ powders treated by non-hydrostatic pressures and temperature treatment was proposed. The Raman spectra of $BaTiO_3$ powder under different non-hydrostatic pressures were measured in the DAC device. To determine the magnitudes of applied non-hydrostatic pressure the Raman line position in the diamond anvil was used. It is shown that the magnitudes of non-hydrostatic pressures applied to the $BaTiO_3$ powder are unambiguously determined by the shift of the Raman line (1332 cm^{-1}) of the diamond anvil.

The relationship between the E(TO) Raman line (307 cm^{-1}) and applied non-hydrostatic pressures in the $BaTiO_3$ powder has been established to determine the magnitudes of residual mechanical stresses.

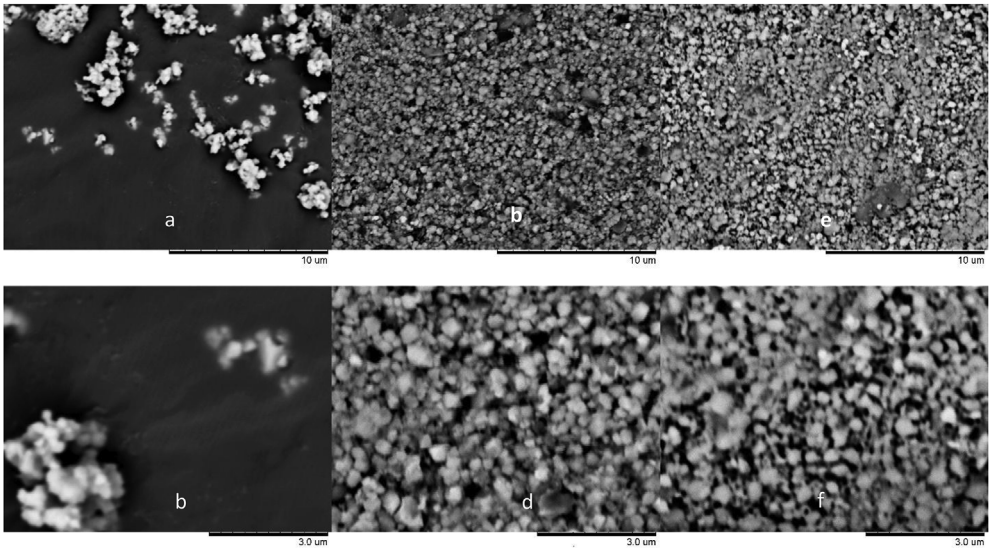

Fig. 6. (a, b) Untreated powder; (c, d) after pressing by 4 GPa; (e, f) after pressing by 4 GPa and annealing at 900°C for 30 min.

To determine the spatial distribution of the residual stresses a position of the 307 cm^{-1} line has measured with a resolution about 0.6 μm in the barium titanate crystal, powder, and the sample obtained by pressing this powder at 4 GPa and temperature annealing of this sample at 900 C to determine the spatial distribution of the residual stresses.

Frequency distributions of some microregions with the same values of the E(TO) line position in the crystal, untreated powder, pressure, and temperature treated powders of the $BaTiO_3$ show that residual mechanical stresses acting in the volume of the pressed powder are distributed relatively uniformly in the micron scale. On the other hand, an increase in width of the Raman line depending on its position may be caused by defects in much smaller scales, up to atomic.

Acknowledgement

The reported study was funded by RFBR according to the research projects No. 17-32-5009, 18-02-00399 and State assignment No AAAA-A17-117052410033-9. The experiments were performed in the multiple-access center “High-Resolution Spectroscopy of Gases and Condensed Matter” in IA&E SBRAS (Novosibirsk, Russia) and Center for Common Use of the Krasnoyarsk Scientific Center, SBRAS (Krasnoyarsk, Russia).

References

[1] G.A. Samara, Pressure and temperature dependences of the dielectric properties of the perovskites $BaTiO_3$ and $SrTiO_3$, Phys. Rev. 151 (1996) 378–386.
[2] W.J. Merz, The effect of hydrostatic pressure on the curie point of barium titanate single crystals, Phys. Rev. 77 (1950) 52–54.
[3] Iniguez Jorge, David Vanderbilt, First-principles study of the temperature-pressure phase diagram of $BaTiO_3$, Phys. Rev. Lett. 89 (2002) 115503.
[4] G.A. Samara, Pressure and temperature dependences of the dielectric properties of the perovskites $BaTiO_3$ and $SrTiO_3$, Phys. Rev. 151 (1966) N 2.
[5] A.M. Pugachev, I.V. Zaytseva, V.I. Kovalevskii, V.K. Malinovsky, N.V. Surovtsev, Yu M. Borzdov, I.P. Raevski, S.I. Raevskaya, M.A. Malitskaya, Local residual stresses in pressure-treated barium titanate powders probed by second harmonic generation, Ferroelectrics 501 (2016) 9–14.
[6] A.M. Pugachev, V.I. Kovalevskii, N.V. Surovtsev, S. Kojima, S.A. Prosandeev, I.P. Raevski, S.I. Raevskaya, Broken local symmetry in paraelectric $BaTiO_3$ proved by second harmonic generation, Phys. Rev. Lett. 108 (2012) 247601.
[7] A.M. Pugachev, I.V. Zaytseva, A.S. Krylov, V.K. Malinovsky, N.V. Surovtsev, Yu M. Borzdov, V. Kovalevsky, Uniaxial mechanical stresses and their influence on the parameters of the ferroelectric phase transition in pressure-treated barium titanate, Ferroelectrics 508 (2017) 161–166.
[8] E.I. Bondarenko, Z.V. Bondarenko, M.V. Lomakov, I.P. Raevskii, Effects of residual mechanical stress on phase transition in hot - pressed ferroelectric ceramics, Sov. Phys. Tech. Phys. 30 (1985) 582–583.
[9] A.M. Pugachev, V.I. Kovalevsky, V.K. Malinovsky, Borzdov YuM, N.V. Surovtsev, Relaxor-like features in pressure-treated barium titanate powder, Appl. Phys. Lett. 107 (2015) 102902.
[10] F. Jona, G. Shirane, Ferroelectric Crystals, Pergamon, London, 1962.
[11] G.A. Samara, Pressure and temperature dependences of the dielectric properties of the perovskites BaTiO3 and SrTiO3, Phys. Rev. 151 (1966) 378–386.
[12] G.A. Samara, Pressure and temperature dependence of the dielectric properties and phase transitions of the ferroelectric perovskites PbTiO, and BaTiO3, Ferroelectrics 2 (1971) 277–289.
[13] W.J. Merz, The effect of hydrostatic pressure on the curie point of barium titanate single crystals, Phys. Rev. 77 (1950) 52–54.
[14] Iniguez Jorge, David Vanderbilt, First-principles study of the temperature-pressure phase diagram of BaTiO3, Phys. Rev. Lett. 89 (2002) 115503.
[15] T. Ishidate, S. Abe, H. Takahashi, N. Mori, Phase diagram of BaTiO3, Phys. Rev. Lett. 78 (1997) 2397–2400.
[16] [Iniguez] Jorge Iniguez and David Vanderbilt, First-principles study of the temperature-pressure phase diagram of BaTiO3, Phys. Rev. Lett. 89 (2002) 1153-1-4.
[17] S.A. Hayward, E.K.H. Salje, The pressure-temperature phase diagram of BaTiO3: a macroscopic description of the low-temperature behaviour, J. Phys. Condens. Matter 14 (2002) L599–L604.
[18] J. Suchanicz, D. Sitko, G. Klimkowski, B. Garbarz-Glos, M. Sokolowski, M. Antonova, A. Sternberg, Influence of uniaxial pressure and aging on dielectric and ferroelectric properties of BaTiO3 ceramics, Phase Transitions 86 (2012) 1–10.
[19] F.H. Schader, E. Aulbach, K.G. Webber, G.A. Rossetti Jr., Influence of uniaxial stress on the ferroelectric-to-paraelectric phase change in barium titanate, J. Appl. Phys. 113 (2013) 174103.
20 E.I. Bondarenko, Z.V. Bondarenko, M.V. Lomakov, I.P. Raevskii, Effects of residual mechanical stress on phase transition in hot - pressed ferroelectric ceramics, Zh. Tekh. Fiz. 55 (1985) 967–969.
[21] H.D. Megaw, Temperature changes in the crystal structure of barium titanium oxide Proc, Phys. Soc. 58 (1946) 133.
[22] H.F. Kay, P. Vousden, Symmetry changes in barium titanate at low temperatures and their relation to its ferroelectric properties, Philosophical Magazine and Journal of Science 40 (309) (1949) 1019–1040.
[23] G. Shirane, A. Takeda Transition, Energy and volume change at three transitions in barium titanat, J. Phys. Soc. Jpn. 7 (1952) 1–4.
[24] D.A. Tenne, P. Turner, J.D. Schmidt, M. Biegalski, Y.L. Li, L.Q. Chen, A. Soukiassian, S. Trolier-McKinstry, D.G. Schlom, X.X. Xi, D.D. Fong, P.H. Fuoss, J.A. Eastman, G.B. Stephenson, C. Thompson, S.K. Streiffer, Ferroelectricity in ultrathin BaTiO3 films: probing the size effect by ultraviolet Raman spectroscopy, Phys.Rev. Let. 103 (2009) 177601-1–177601-177604.
[25] K.J. Choi, 1 M. Biegalski, Y.L. Li, A. Sharan, J. Schubert, R. Uecker, P. Reiche, Y.B. Chen, X.Q. Pan, V. Gopalan, L.-Q. Chen, D.G. Schlom, C.B. Eom, Enhancement of ferroelectricity in strained BaTiO3 thin films, Science 306 (2004).
[26] Oswaldo Diéguez, Silvia Tinte, A. Antons, Claudia Bungaro, J.B. Neaton, Karin M. Rabe, David Vanderbilt, Ab initio study of the phase diagram of epitaxial BaTiO3, Phys. Rev. B 69 (2004) 212101.
[27] A.M. Pugachev, V.K. Malinovsky, N.V. Surovtsev, YuM. Borzdov, I.P. Raevskii, S.I. Raevskaya, M.A. Malitskaya, Local residual stresses in pressure-treated barium titanate powders probed by inelastic light scattering, Ferroelectrics 496 (2016) 225–230.
[28] W. Zhang, L. Chen, C. Jin, X. Deng, X. Wang, L. Li, High pressure Raman studies of dense nanocrystalline $BaTiO_3$ceramic, J. Electroceram. 21 (2008) 859–862.
[29] A.M. Pugachev, I.V. Zaytseva, A.S. Krylov, V.K. Malinovsky, N.V. Surovtsev, Yu M. Borzdov, V. Kovalevsky, Uniaxial mechanical stresses and their influence on the parameters of the ferroelectric phase transition in pressure-treated barium titanate, Ferroelectrics 508 (2017) 161–166.
[30] F. Datchi, R. LeToullec, P. Loubeyre, Improved calibration of the $SrBr_4O_7:Sm^{2+}$

optical pressure gauge: advantages at very high pressures and high temperatures, J. Appl. Phys. 81 (1997) 3333.
[31] Datchi, A. Dewaele, P. Loubeyre, R. Letoullec, Y. Le Godec, B. Canny, Optical pressure sensors for high-pressure–high-temperature studies in a diamond anvil cell, High Press. Res. 27 (4) (2007) 447–463.
[32] K.A. Okotrub, N.V. Surovtsev, Redox state of cytochromes in frozen yeast cells probed by resonance Raman spectroscopy, Biophys. J. 109 (2015) 2227–2234.
[33] Yuichi Akahama, Haruki Kawamura, Pressure calibration of diamond anvil Raman gauge to 410 GPa, J. Phys. Conf. Ser. 215 (2010) 012195.
[34] Yuichi Akahama, Haruki Kawamura, High-pressure Raman spectroscopy of diamond anvils to 250GPa250GPa: Method for pressure determination in the multimegabar pressure range, J. Appl. Phys. 96 (7) (2004).
[35] M. Hanfland, K. Syassen, A Raman study of diamond anvils under stress, J. Appl. Phys. 57 (1985) 2752.
[36] Shigeaki Ono, Kenji Mibe, Ohishi Yasuo, Raman spectra of culet face of diamond anvils and application as optical pressure sensor to high temperatures, J. Appl. Phys. 116 (2014) 053517.
[37] Y.J. Jiang, L.Z. Zeng, R.P. Wang, Y. Zu, Y.L. Liu, Fundamental and second order Raman spectra of BaTiO3, J. Raman Spectrosc. 27 (1996) 31–34.
[38] S.A. Hayward, E.K.H. Salje, The pressure-temperature phase diagram of BaTiO3: a macroscopic description of the low-temperature behaviour, J. Phys. Condens. Matter 14 (2002) L599–L604.
[39] N.V. Surovtsev, I.N. Kupriyanov, V.K. Malinovsky, V.A. Gusev, Yu N. Pal'yanov, Effect of nitrogen impurities on the Raman line width in diamonds, J. Phys. Condens. Matter 11 (1999) 4767–4774.